Optimization of Friction Stir Welding Operation Using Optimal Taguchi-based ANFIS and Genetic Algorithm

An-Le Van[1] – Trung-Thanh Nguyen[2,*]

[1]Nguyen Tat Thanh University, Faculty of Engineering and Technology, Vietnam
[2]Le Quy Don Technical University, Faculty of Mechanical Engineering, Vietnam

The friction stir welding (FSW) process is an effective approach to producing joints of superior quality. Unfortunately, most published investigations primarily addressed optimizing process parameters to boost product quality. In the current work, the FSW operation of an aluminium alloy has been considered and optimized to decrease the specific welding energy (SWE) and enhance the jointing efficiency (JE) as well as micro-hardness at the welded zone (MH). The parameter inputs are the rotational speed (S), welding speed (f), depth of penetration (D), and tool title angle (T). The optimal adaptive neuro-based-fuzzy inference system (ANFIS) models were utilized to propose the welding responses in terms of the FSW parameters, while the Taguchi method was applied to optimize the ANFIS operating parameters. The neighbourhood cultivation genetic algorithm (NCGA) was employed to determine the best solution. The obtained results indicated that the optimal values of the S, f, D, and T are 560 rpm, 90 mm/min, 0.9 mm, and 2 deg, respectively. The SWE is decreased by 17 %, while the JE and MH are improved by 2.3 % and 6.4 %, respectively, at the optimal solution. The optimal ANFIS models for the welding responses were adequate and reliably employed to forecast the response values. The proposed optimization approach comprising the orthogonal array-based ANFIS, Taguchi, and NCGA could be effectively and efficiently utilized to save experimental costs as well as human efforts, produce optimal predictive models, and select optimum outcomes. The observed findings contributed significant data to determine optimal FSW parameters and enhance welding responses.
Keywords: friction stir welding; energy efficiency; jointing efficiency; micro-hardness; NCGA

Highlights
- *FSW operating parameters, including the rotational speed, welding speed, depth of penetration, and tool title angle were considered.*
- *The specific welding energy was minimized, while the jointing efficiency and micro-hardness at the welded zone were maximized.*
- *Optimal orthogonal array-based ANFIS models for welding performances were developed.*
- *An efficient optimization approach comprising the ANFIS, Taguchi, and NCGA was proposed.*

0 INTRODUCTION

The friction stir welding (FSW) operation is an effective and efficient solid-state joining process in which the tool plastically deforms the material and mixes it to produce strong welds. The FSW process is widely employed to avoid the porosity, hot crack, and large deformation due to non-material melting, as compared to the other fusion welding processes. Moreover, this technology does not require material, such as shielding gas, electrodes, and filling materials, for generating welded joints. Consequently, the FSW operation could be efficiently and effectively applied to produce high quality joints for different materials with similar and/or dissimilar thicknesses.

Many attempts have been executed to improve the mechanical properties of the joints for different FSW operations, in which the conventional welding responses are the ultimate tensile strength (*TS*), yield strength (*YS*), elongation (*EL*), welding force (*WF*), welding temperature (*WT*), micro-hardness at the welded zone (*MH*), and grain size (*GS*). The ratio

between shoulder and pin diameters (*R*) of 4, the rotational speed (*S*) of 100 rpm, the welding speed (*f*) of 100 mm/min were utilized to improve the *TS* and *EL* of the AA6082-AA5754 joint [1]. The pin square, the *S* of 1400 rpm, the *f* of 1.75 mm/s, and the axial force (*AF*) of 7.5 KN were applied to enhance the *TS*, *MH*, and *YS* of the AA7075 weld [2]. The optimal data of the *f*, *S*, and *T* were 25 mm/min, 1250 rpm, and 1 deg, respectively, which could be used to obtain the *TS* of 6.06 MPa for the composite joint [3]. Shojaeefard et al. stated that the optimal values of the *S* and *f* for the FSW operation of AA5083 were 1345 rpm and 60.0 mm/min, respectively [4]. For the welded magnesium alloy, the *S* was found to be the most effective contribution, followed by the *f* and the *AF* [5]. The *S* of 1550 rpm, the *T* of 4 deg, and octagonal pin were applied to boost the *TS* and *EL* of the aluminium alloy weld [6]. Gou et al. emphasized that the maximum *TS* and *MH* for the AA6061-T6 could be obtained at the *D* of 0.45 mm [7]. Saju and Narayanan revealed that the highest mechanical properties of the AA5052-AA6061 weld were achieved with the *D* of 0.6 mm [8]. The *TS* of 2.6 KN and the *MH* of 70.45 HV

*Corr. Author's Address: Le Quy Don Technical University, 236 Hoang Quoc Viet, Ha Noi, VietNam, trungthanhnguyen@lqdtu.edu.vn

for the dissimilar AA5083-C10100 weld were obtained at the S of 1250 rpm, depth of penetration (D) of 1.9 mm, and dwell time (DT) of 12.5 s, respectively [9]. Elyasi et al. emphasized that the T of 2 deg could be applied to improve the TS and MH of the AA1100 weld [10]. Farzadi et al. indicated that the S of 513 rpm, the f of 95 mm/min, the shoulder diameter (SD) of 16.1 mm and the D of 5 mm could be applied to maximize the TS of the AA7075 weld [11]. The S of 900 rpm, f of 60 mm/min, SD of 18 mm, and D of 5 mm were employed to enhance the TS, MH, and GS for the AA5083-AA6063 weld [12].

Palanivel et al. indicated that the S of 1000 rpm, the f of 60 mm/min, and the partial impeller pin were applied to improve the TS of AA6351-AA5083 joint [13]. The vertical force model of the FSW operation of AZ31 magnesium alloy was developed with the aid of an artificial neural network (ANN) [14]. Rajendran et al. revealed that the defect-free welds were obtained using the T of 1 deg to 3 deg [15]. The S of 1005 rpm, f of 20 mm/min, and T of 3 deg were utilized to increase the TS of the AA2219 joint [16]. The TS of 167 MPa, the YS of 145 MPa, and the EL of 8.3 % for the 6063-T6 joint were achieved using optimum outcomes [17]. The maximum TS (135.83 MPa) and EL (4.35 %) of the AAA6061-A5083 joint were produced at the T of 1.11 deg, the S of 1568 rpm, and the f of 39.53 mm/min, respectively [18]. Boukraa et al. indicated that the WT and dissolution time were enhanced by 13.44 % and 46.5 %, respectively, at the optimal solution for the AA2195-T8 joint [19]. Satheesh et al. revealed that the taper cylindrical pin geometry, the S of 1045 rpm, the f of 1.5 mm/s, and the AF of 4.87 kN were applied to improve the TS, YS, and EL for the AZ91C Mg alloy joint [20]. The distribution of the WT on the AZ80A Mg Alloy joint was analysed by Sevvel et al., in which the authors stated that the S was named as the best contribution, followed by the f and AF, respectively [21]. The empirical models of the TS, EL, and percentage reduction in area were developed in terms of the S, f, and SD for the carbon steel weld [22]. A simulation model was developed to investigate the impacts of the S and pin geometry on the WT for the AZ80A Mg alloy weld, in which the authors stated that the maximum WT was obtained by means of distinctive geometries [23].

As a result, different FSW processes with various materials have been considered and optimized to enhance welding performances. However, the shortcomings of published works can be listed as follows.

Quality indicators are primary considerations of the aforementioned works. The impacts of FSW factors on energy consumption have not been analysed.

The energy consumption model regarding the FSW parameters has not been developed.

The selection of optimal FSW parameters for decreasing energy consumed and improving the welding quality (e.g., ultimate tensile strength and elongation) has not been addressed.

To overcome these challenges, the FSW operation of the AA6061 has been considered and optimized to decrease the specific welding energy (SWE) and enhance the jointing efficiency (JE) as well as micro-hardness at the welded zone (MH). The optimal Taguchi-based ANFIS models were utilized to propose FSW performances regarding the S, f, D, and T. The optimal outcomes are selected with the aid of the NCGA.

The scientific contributions of the current study can be expressed as follows.

The developed optimizing method comprising the Taguchi method, ANFIS, and NCGA can be considered an effective and efficient approach to solving complicated optimization issues and selecting optimal outcomes. The developed approach possesses various advantages, including low experimental costs, decreased human efforts, and easy implementation. The developed technique could be effectively and efficiently employed to optimize not only welding operations but also other machining processes.

The impacts of the FSW parameters on the FSW responses have been thoroughly analysed. The obtained knowledge can help machine operators comprehend the physical insights in the FSW operation of the AA6061.

The analysed outcomes of the current study can be effectively and efficiently utilized as significant references for future investigations and developing expert systems regarding FSW processes.

1 OPTIMIZING FRAMEWORK

Traditionally, the primary aim of the FSW process is to produce the welds with superior quality, as seen in factors such as ultimate tensile strength, elongation, micro-hardness at the weld nugget zone, yield strength, and grain size. Unfortunately, the rise of energy cost and environmental legislation requires manufacturers to decrease energy consumed, welding noise/fumes, and wastage. In this investigation, three technological responses, including the SWE, JE, and MH, are listed as important indicators.

The profile of the power consumed for the FSW process is shown in Fig. 1, in which three operating

phases, including the plunge, dwell, and welding states are depicted. For the plunge phase, the workpieces are tightly clamped on the fixture, while the rotating tool is inserted into the joint line of plates. For the dwell phase, the rotational motion of the welding tool is kept in its position to plasticize the material around the pin. For the welding phase, the linear motion of the tool is performed to produce the weld in the solid state.
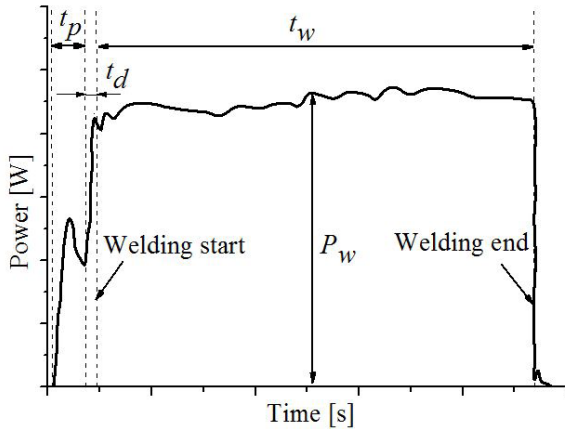
Fig. 1. *The profile of the power consumption*

The *SWE* value is calculated as:

$$SWE = \frac{P_w}{f}, \qquad (1)$$

where P_w and f are the power consumed in the welding time and welding speed, respectively.

The *JE* value is computed as:

$$JF = \frac{UTS_w}{UTS_b}, \qquad (2)$$

where UTS_w and UTS_b denote the ultimate tensile strength of the weld and base material, respectively.

The *MH* value is computed as:

$$MH = \frac{\sum_{i=1}^{n} MH_i}{n}, \qquad (3)$$

where MH_i and n denotes the micro-hardness at the ith position and the number of measuring points, respectively.

The schematic of the FSW operation with the four process parameters is shown in Fig. 2. The welding tool and materials used are considered fixed conditions. Four key process parameters, including the *S*, *f*, *D*, and *T* are listed as optimizing inputs (Table 1). The ranges of the *S* and *f* are primarily selected based on the specifications of the machine tool and recommendations of the manufacturer of the welding

tool. The levels of the *D* and *T* are determined using the configuration of the machine tool and the knowledge of the previous publications. The highest and lowest values of process parameters were tested by means of experimental trials to ensure machinability. These values are confirmed by company experts and welding handbooks.
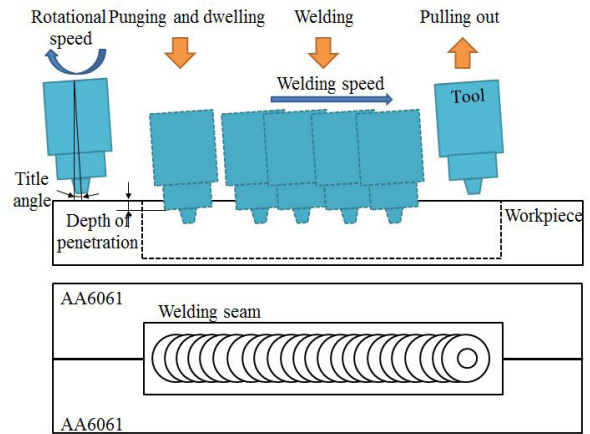
Fig. 2. *The schematic illustration of the FSW operation*

Consequently, the optimizing issue is expressed as follows:

Finding $X = [S, f, D,$ and $T]$.

Maximizing *JE* and *MH*; Minimizing *SWE*.

Constraints: $480 \leq S \leq 1600$ rpm;
$48 \leq f \leq 112$ mm/min; $0.6 \leq D \leq 1.2$ mm; $0 \leq T \leq 4$ deg

The systematic approach for generating optimal FSW parameters is shown in Fig. 3.

Step 1: The physical experiments of the FSW operation are then conducted using the orthogonal array L_{32}.

Step 2: The ANFIS models of the *SWE*, *JE*, and *MH* are developed in terms of the FSW parameters. In this investigation, the ANFIS with five layers are developed to model welding performances [24].

Layer I: This layer is employed to convert the inputs set to fuzzy set with the aid of the assigned membership function. The outputs of three welding responses are expressed:

$$L1, x = \mu Ax(E), \qquad (4)$$

$$L1, y = \mu By(T), \qquad (5)$$

$$L1, z = \mu Cz(L), \qquad (6)$$

where *E*, *T*, and *L* are the input variable nodes, while *x*,

y, *z*, *A*, *B*, and *C* are connected labels having $\mu(E)$, $\mu(S)$, and $\mu(P)$ as memberships.

Layer II: This layer is employed to generate the fixed function of the input. The node function Π is expressed as:

$$L2, x = \mu Ax(E) \times \mu By(T) \times \mu Cz(L). \tag{7}$$

Layer III: This layer contains the fixed node labelled N. The output namely the normalized firing strength is represented as:

$$L3x = \overline{\omega_i} = \frac{\omega_i}{\sum_{i=1}^{n} \omega_i}. \tag{8}$$

Layer IV: This layer contains an adaptive node. The current layer is applied to assign the consequent parameters of the rules. The output of this layer is expressed as:

$$L4x = \overline{\omega_i}(a_i x + b_i x + c_i), \tag{9}$$

where a_i, b_i, and c_i are the consequent parameters, respectively.

Layer V: This layer comprises only one fixed node. The fifth layer is used to calculate the overall output of all incoming signals. The output of this layer is expressed as:

$$L5x = \sum_i \overline{\omega_i} f_i. \tag{10}$$

Step 3: The optimal parameters of the ANFIS models are selected using the Taguchi method.

It is necessary to select the proper operating factors of each ANFIS model to minimize the predictive errors. The aforementioned publications randomly determine the operating parameters, including the number of inputs, types of input, optimal method, and types of output. Practically, a variety of each ANFIS parameter changes the mean square error (MSE), which is expressed as:

$$MSE = \frac{1}{n} \sum_{i=1}^{n} (y_m - y_p)^2, \tag{11}$$

where y_m and y_p are the measured and predicted values, respectively.

Step 4: The optimal outcomes of the FSW process factors and technical responses are selected with the aid of the NCGA.

The NCGA is an effective solution to solve the trade-off analysis between the conflicting responses. This algorithm possesses various advantages, including easy computational skills, a large number of feasible solutions, and producing global optimization results. The NCGA provides better results than conventional approaches, such as multi-objective genetic algorithm (MOGA) and non-dominated sorting genetic algorithm II (NSGA-II) when responses have a multiple peak landscape and a higher number of design variables. However, the NCGA requires higher computational time to conduct the algorithm. The working principle of the NCGA is summarized, as follows (Fig. 4):

- Assigning initial population (P_0) and computing fitness of the initial individual.
- Generating and sorting a new generation (P_t) based on the objective purpose.
- Performing crossover and mutation operations for generating new child individuals.
- Assembling produced individuals and generating a new population.
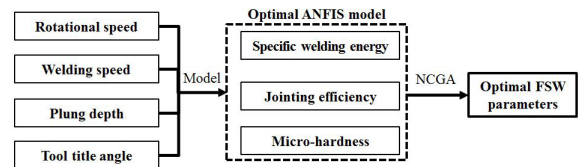
Fig. 3. *The flow chart of optimization approach*

Table 1. *FSW parameters for the experimental work*

No.	Symbol	Parameters	Values		
1	*S*	Rotational speed [rpm]	480	1120	1600
2	*f*	Welding speed [mm/min]	48	77	112
3	*D*	Depth of penetration [mm]	0.60	0.90	1.20
4	*T*	Tool title angle [deg]	0	2	4

2 EXPERIMENTS AND MEASUREMENTS

The welding specimens with a length of 160 mm, a width of 100 mm, and a thickness of 6 mm are prepared with the aid of milling process. The joints between the AA6061 plates are widely utilized in the marine industry to resist the corrosion of seawater. The chemical compositions and mechanical properties of the AA6061 with the aid of the axial tension test are presented in Table 2.

The welding experiments are done with the aid of a vertical milling machine and a fabricated fixture (Fig. 5). The welding tool with a cylindrical tapered pin is applied to perform trials. The hot die steel entitled H13 is used as the tool material due to its high strength, wear resistance, and stability at higher temperatures. The flat bars are employed to clamp the workpiece tightly using the bolts.
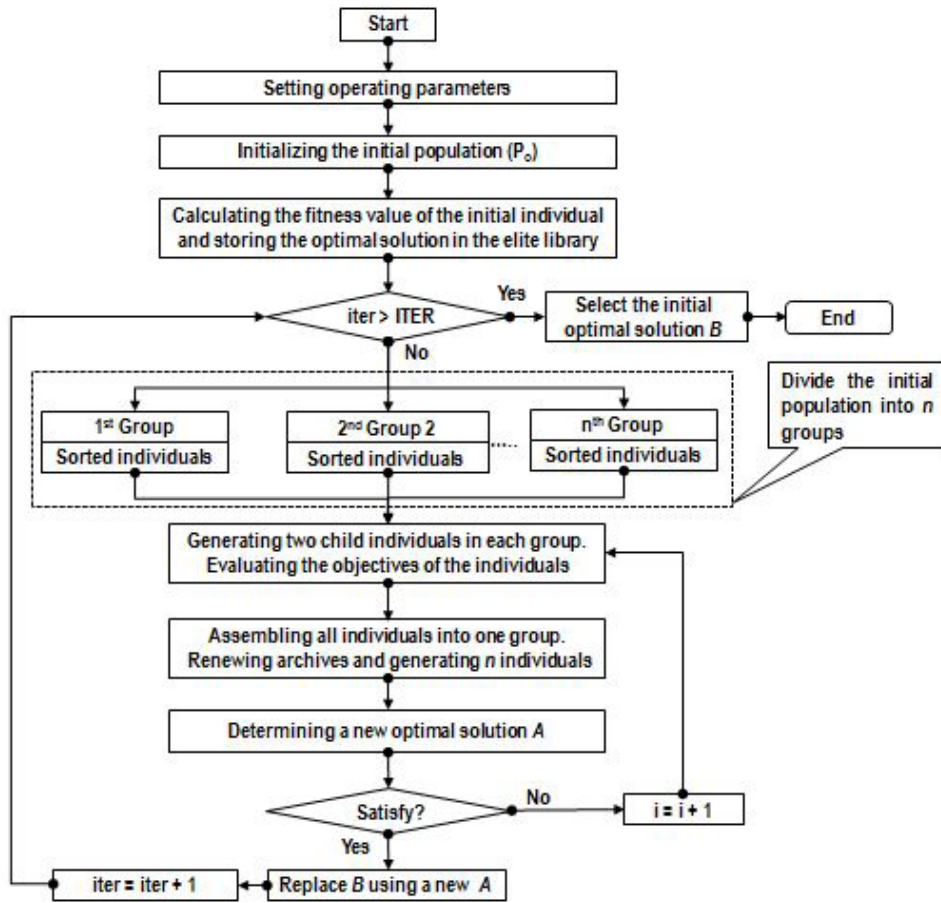
Fig. 4. *The operating principle of the NCGA*

Table 2. *Chemical compositions and mechanical properties of the AA6061*

Element	Mn	Fe	Mg	Si	Cu	Zn	Ti	Cr	Others	Al
[%]	0.12	0.55	0.10	0.60	0.30	0.20	0.10	0.30	0.10	Balance

Mechanical properties					
Ultimate tensile strength [MPa]	Yield stress [MPa]	Elongation [%]	Vickers Hardness [HV]	Poisson's ratio	Modulus of elasticity [GPa]
241	214	15.2	104	0.33	68.9

A power sensor (Kyoritsu 6305) is used to record the variety of power components during the welding time. The obtained data is stored in the flashcard and visualized with the aid of the KEW6305 software. The reading and scaling errors are ±0.3 % and ±0.2 %, respectively, to improve the measuring precision, while the up-dating time of 1 second is utilized to visualize the capture data.

The ultimate tensile strength and elongation are obtained with the aid of the Exceed E45 machine based on the American Society for Testing of Materials (ASTM E8) guidelines. The resolution of 0.1 MPa is employed to improve the accuracy of

the measuring tensile strength. The Vickers Wolperts Wilson machine is used to measure the micro-hardness with the force of 500d at the dwell time of 20 seconds. The resolution of 0.1 HV is applied to capture the experimental data.

3 RESULTS AND DISCUSSION

3.1 Development of the Optimal ANFIS Models

The experimental outcomes of the FSW operation are shown in Table 3.
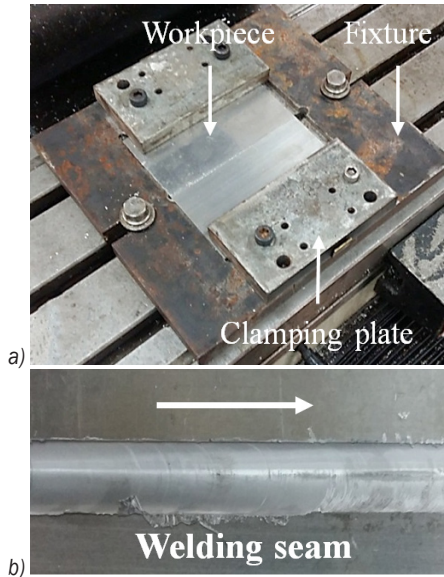
Fig. 5. *FSW Experiment; a) experimental setting, b) representative specimen*

Practically, the optimal architecture of the ANFIS model is randomly determined using the decisive maker, which decreases the predicting precision. In this study, optimal Taguchi-based ANFIS models are proposed to render the relations between process parameters and FSW performances. Four ANFIS operating parameters are the number of input MFs (N), types of input MFs (TI), optimal method (O), and types of output MFs (TO). The parameter combinations of the ANFIS model are produced with the support of the Taguchi experimental matrix L_{16}. The numerical experiments of ANFIS models are executed to calculate the MSE values for three welding responses. As shown in Fig. 6a, the optimal outcomes of the N, TI, O, and TO for the *SWE* model are 2, *gaussmf*, *hybrid*, and *linear*, respectively. As shown in Figs. 6b and c, the optimal outcomes of the N, TI, O, and TO for the *JE* and *MH* models are 2, *gaussmf*, *hybrid*, and *constant*, respectively. The 2-2-2-2-2 ANFIS architecture can be used to render the relations between welding parameters and the responses (Fig. 7). The schematic rules for ANFIS models of the *SWE, JE*, and *MH* are shown in Figs. 8 a, b, and c, respectively.

The Gaussian membership function is expressed as:

$$\mu_{Ai}(x) = \exp\left[-\frac{1}{2}\left(\frac{x - c_i}{a_i}\right)^2\right], \quad (12)$$

where a_i and c_i are the definite centre and its width of the membership function, respectively.

To investigate the accuracy of developed ANFIS models, a set of experiments is performed at random points. The comparisons between the obtained and ANFIS results are presented in Table 4. The errors of the *SWE, JE*, and *MH* lie within the range of -1.48 % to 0.53 %, -0.86 % to 0.59 %, and -0.11 % to 1.20 %, respectively. The accepted deviations indicate that the developed models performed well in predicting welding responses.
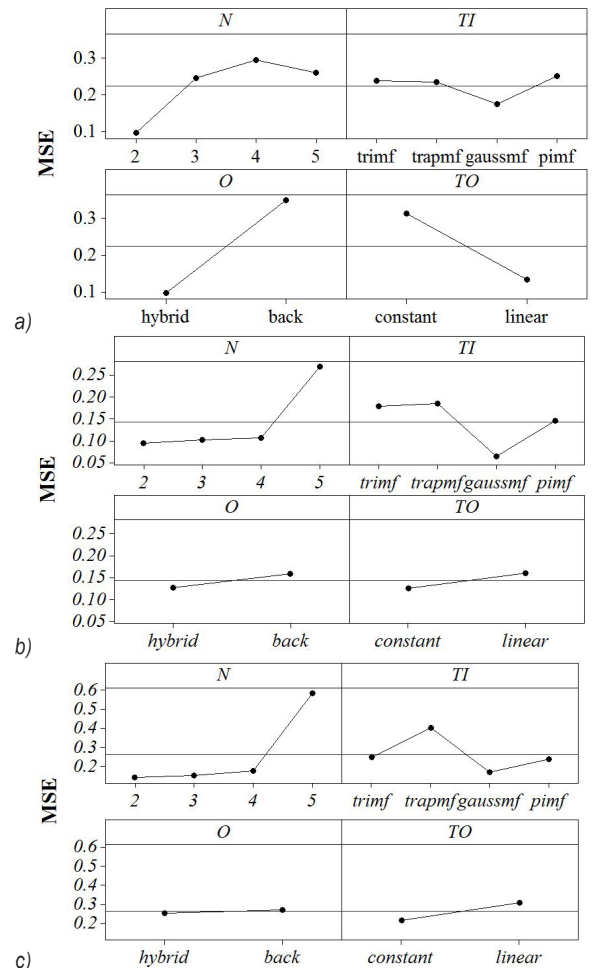
Fig. 6. *MSE values for FSW responses; a) for SWE model, b) for JE model, c) for MH model*

3.2 ANOVA Results for Welding Performances

The ANOVA results of the SWE, JE, and MH models are presented in Tables 5 to 7, respectively. The R^2, adjusted R^2, and predicted R^2 values indicate that the developed models are adequate.
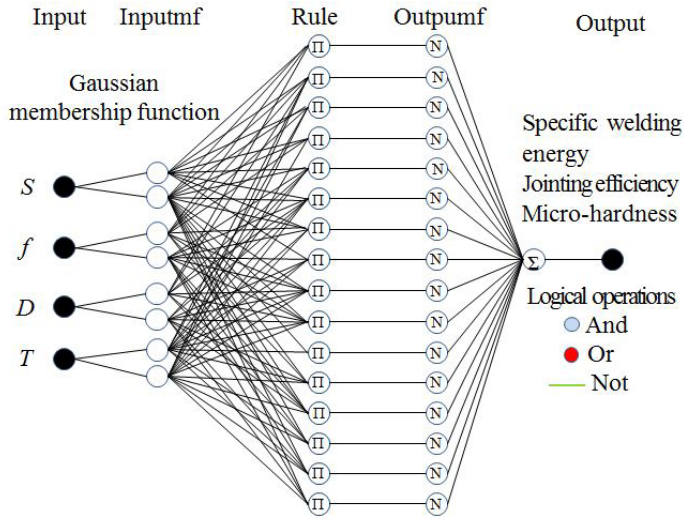
Fig. 7. *The ANFIS structures for welding performances*

Table 3. *Experimental data for the FSW operation*

	No.	S [rpm]	f [mm/min]	D [mm]	T [deg]	SWE [J/mm]	UTS$_w$ [MPa]	JE [%]	MH [HV]
	1	480	48	0.6	0	1693.64	133.1	55.24	74.2
	2	1120	77	0.6	2	1211.24	158.9	65.95	62.8
	3	1600	112	0.6	4	960.73	131.2	54.45	60.3
	4	480	48	0.6	0	1693.64	133.2	55.28	74.2
	5	480	48	0.6	2	1741.24	152.7	63.36	71.4
	6	1120	77	0.6	0	1175.54	139.5	57.89	66.2
	7	1600	112	0.6	0	909.19	113.8	47.22	69.3
	8	480	48	0.6	4	1801.61	151.1	62.68	66.7
	9	480	77	0.9	4	1255.48	151.3	62.78	62.8
	10	1120	48	0.9	0	1903.33	165.0	68.45	55.3
	11	1600	48	0.9	0	2013.54	164.3	68.17	51.1
	12	480	112	0.9	2	889.28	139.2	57.78	72.4
	13	480	77	0.9	0	1183.62	142.1	58.98	68.3
Experimental	14	1120	48	0.9	4	2016.12	174.1	72.22	47.5
data for	15	1600	48	0.9	2	2066.76	179.5	74.48	47.5
developing the	16	480	112	0.9	0	879.27	124.2	51.53	73.8
ANFIS models	17	480	48	1.2	0	1854.52	160.3	66.53	61.2
of welding	18	1120	112	1.2	2	934.86	161.1	66.83	60.4
responses	19	1600	77	1.2	4	1461.78	170.3	70.67	43.9
	20	480	48	1.2	0	1854.52	160.5	66.58	61.2
	21	480	48	1.2	2	1898.37	171.3	71.08	59.9
	22	1120	112	1.2	0	922.43	150.3	62.36	62.2
	23	1600	77	1.2	0	1378.67	169.9	70.49	51.1
	24	480	48	1.2	4	1954.99	161.1	66.86	56.5
	25	480	112	0.6	4	860.74	126.4	52.45	74.4
	26	1120	48	0.6	0	1800.72	147.8	61.31	63.5
	27	1600	48	0.6	0	1910.77	145.7	60.44	59.2
	28	480	77	0.6	2	1134.09	146.3	60.71	73.5
	29	480	112	0.6	0	824.22	108.9	45.17	80.7
	30	1120	48	0.6	4	1917.26	165.6	68.73	54.2
	31	1600	48	0.6	2	1965.87	165.2	68.54	54.9
	32	480	77	0.6	0	1102.67	126.8	52.63	75.9
Experimental	33	560	66	0.8	2	1397.78	160.3	66.52	65.7
data for testing	34	800	90	1.0	0	1052.33	150.1	62.28	63.1
the accuracy	35	1250	112	1.2	4	973.83	151.1	62.68	55.3
of developed	36	1600	66	0.9	0	1557.83	159.2	66.05	53.4
ANFIS models	37	1250	90	1.1	4	1178.58	164.2	68.15	50.2
	38	1120	90	1.0	4	1151.58	162.1	67.27	52.6

Table 4. *Comparative errors for the welding responses*

No.	SWE [J/mm]			JE [%]			MH [HV]		
	Exp.	ANFIS	Err. [%]	Exp.	ANFIS	Err. [%]	Exp.	ANFIS	Err. [%]
33	1397.78	1390.42	0.53	66.52	66.14	0.57	65.7	65.2	0.76
34	1052.33	1067.89	-1.48	62.28	62.77	-0.79	63.1	63.8	-1.11
35	973.83	970.12	0.38	62.65	62.28	0.59	55.3	55.7	-0.72
36	1557.83	1552.94	0.31	66.05	66.62	-0.86	53.4	53.8	-0.75
37	1178.58	1172.93	0.48	68.15	68.73	-0.85	50.2	49.6	1.20
38	1151.58	1159.46	-0.68	67.27	67.59	-0.48	52.6	52.1	0.95

Exp.: Experimental value; Err.: Error

For the SWE model, single terms (S, f, D, and T), interactive terms (Sf, fD, and fT), and quadratic terms (S^2, f^2, and D^2) are significant factors. The contributions of the S, f, D, and T are 7.89 %, 50.59 %, 5.47 %, and 3.77 %, respectively. The contributions of the Sf, fD, and fT are 3.28 %, 2.35 %, and 1.77 %, respectively. The contributions of the S^2, f^2, and D^2 are 1.73 %, 19.74 %, and 2.18 %, respectively.

For the JE model, single terms (S, f, D, and T), interactive term (Sf, SD, and DT), and quadratic terms (S^2, f^2, D^2, and T^2) are significant factors. The contributions of the S, f, D, and T are 8.81 %, 20.64 %, 16.09 %, and 6.64 %, respectively. The contributions of the Sf, SD, and DT are 2.78 %, 2.46 %, and 6.29 %, respectively. The contributions of the S^2, f^2, D^2, and T^2 are 11.16 %, 6.93 %, 2.45 %, and 15.52 %, respectively.

For the MH model, single terms (S, f, D, and T), interactive term (Sf, ST, fD, and DT), and quadratic terms (S^2, f^2, D^2, and T^2) are significant factors. The contributions of the S, f, D, and T are 23.89 %, 16.87 %, 16.49 %, and 11.49 %, respectively. The contributions of the Sf, ST, fD, and DT are 2.94 %, 2.53 %, 2.29 %, and 2.29 %, respectively. The contributions of the S^2, f^2, D^2 and, T^2 are 7.18 %, 3.86 %, 5.66 %, and 3.37 %, respectively.

3.3 The Impacts of FSW Parameters

The influences of FSW parameters on the specific welding energy are shown in Fig. 9.

Fig. 9a indicates that a higher S increases the SWE, while an increased f causes a reduction in the SWE. When the S relatively rises from 480 rpm to 1600 rpm, the SWE is relatively increased by 13.6 %. At a higher S, the momentum of the main spindle increases and the spindle system consumes more power consumed to satisfy the desired value. The total power consumed of the machine tool increases; hence, the SWE increases according to Eq. (1). An increased S causes higher welding engagement between the tool and

Table 5. *ANOVA results for the SWE model*

So	SS	MS	F Value	p-value
Mo	343725.7	343725.7	35.3	0.0001
S	598793.7	598793.7	859.8	0.0001
f	383216.9	383216.9	5512.8	0.0001
D	415233.3	415233.3	596.1	0.0001
T	286087.7	286087.7	410.8	0.0001
Sf	248222.2	248222.2	357.4	0.0033
fD	178436.6	178436.6	256.1	0.0046
fT	134269.3	134269.3	192.9	0.0058
S2	131912.9	131912.9	188.5	0.0062
f2	149067.7	149067.7	2151.1	0.0001
D2	164422.1	164422.1	237.5	0.0048
Res	76608.1	6964.4		
Cor	351433.8			

$R^2 = 0.9782$; Adjusted $R^2 = 0.9734$; Predicted $R^2 = 0.9622$

Table 6. *ANOVA results for JE model*

So	SS	MS	F Value	p-value
Mo	892.76	63.769	41.008	< 0.0001
S	26533.5	26533.5	17063.37	< 0.0001
f	62162.5	62162.5	39975.93	< 0.0001
D	48459.1	48459.1	31163.41	< 0.0001
T	199981	199981	12860.47	< 0.0001
Sf	8372.6	8372.6	5384.35	0.0045
SD	7408.9	7408.9	4764.57	0.0048
DT	18943.9	18943.9	12182.58	0.0003
S2	33611.1	33611.1	21614.89	< 0.0001
f2	20871.4	20871.4	13422.15	0.0001
D2	7378.7	7378.7	4745.205	0.0048
T2	46742.4	46742.4	30059.42	< 0.0001
Res	17.105	1.555		
Cor	909.865			

$R^2 = 0.9812$; Adjusted $R^2 = 0.9746$; Predicted $R^2 = 0.9622$

workpiece to be machined, leading to higher friction at the interfaces. Greater resistance is produced, which requires more power used to overcome the friction of the joining materials; hence, the SWE logically increases. There are similar impacts of the spindle

a)

b)

c)

Fig. 8. *The schematic rules for;*
a) SWE model, b) IF model, and c) MH model

Table 7. *ANOVA results for MH model*

So	SS	MS	F Value	p-value
Mo	1446.74	103.34	33.081	< 0.0001
S	1639.87	1639.87	524.963	< 0.0001
f	1158.00	1158.00	370.705	< 0.0001
D	113.91	113.91	362.354	< 0.0001
T	788.70	788.70	252.483	< 0.0001
Sf	201.81	201.81	64.604	0.0056
ST	173.66	173.66	55.595	0.0058
fD	157.19	157.19	50.321	0.0061
DT	157.19	157.19	50.321	0.0061
S2	492.85	492.85	157.775	0.0002
f2	264.96	264.96	84.820	0.0043
D2	388.51	388.51	124.374	0.0003
T2	231.32	231.32	74.053	0.0044
Res	34.36	3.12		
Cor	1481.10			

$R^2 = 0.9768$; Adjusted $R^2 = 0.9691$; Predicted $R^2 = 0.9638$

Fortunately, the *SWE* is inversely proportional to *f* according to Eq.1; therefore, higher *f* decreases the *SWE* value. An increment in the *f* causes a reduction in the welding time, which decreases the machining engagement between the tool and workpiece; hence, a decreased friction at the interfaces is obtained. Low power consumption is required due to low resistance; hence, the *SWE* decreases. Similar impacts of the transverse speed on the energy consumption can be found in the turning [25], milling [26], and burnishing [27] operations.

As shown in Fig. 9b, an increased *D* causes a higher *SWE*. When the *D* relatively changes from 0.6 mm to 1.2 mm, the *SWE* is relatively increased by 9.6 %. An increase in the *D* causes a higher depth of shoulder inside the workpiece. This creates hindrances for tool movement, leading to higher friction at the interfaces between the tool and workpiece. Higher power consumed is required to overcome greater resistance; hence, the *SWE* increases. An increased energy consumption with a higher depth of penetration can be found for the turning [25], milling [26], and burnishing [27] processes.

As shown in Fig. 9b, an increased *T* causes a higher *SWE*. When the *T* relatively rises from 0 deg mm to 4 deg, the *SWE* is relatively increased by 6.3 %. At a higher *T*, the depth of the shoulder inside the specimen increases; which leads to higher friction between the tool and workpiece. Greater resistance for tool movement is obtained, which requires more power consumption; hence, a higher *SWE* is required. Higher energy consumption with an increased *T* was presented in the work of [10].

speed on the energy consumption for the turning [25], milling [26], and burnishing [27] processes.

As shown in Fig. 9a, when the *f* relatively changes from 47 mm/min to 112 mm/min, the *SWE* is relatively decreased by 52.6 %. An increased *f* causes higher power consumption in the feed driving system; hence, the total power used in the machine tool increases.

a)

b)
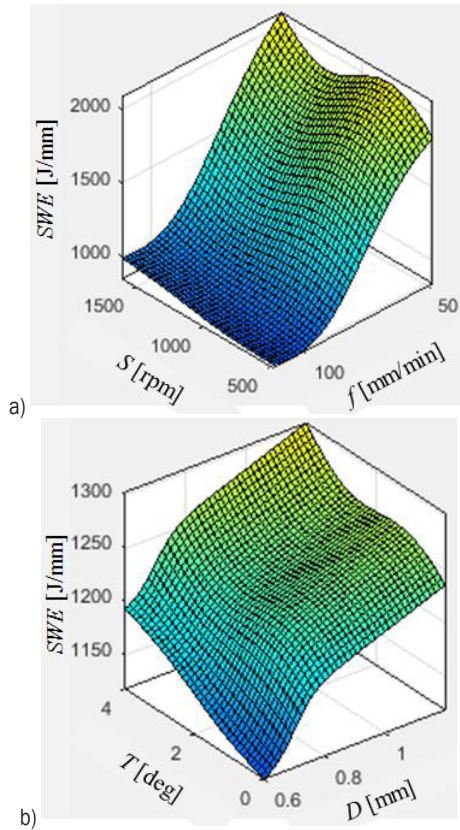
Fig. 9. *The interactive influences; a) SWE versus S and f, and b) SWE versus T and D*

The influences of FSW parameters on the jointing efficiency are shown in Fig. 10. As shown in Fig. 10a, the *JE* increases as the *S* increases to the middle value and decreases thereon. When the *S* rises from 480 rpm to 1120 rpm, the *JE* is relatively increased by 8.4 %. The *JE* is relatively decreased by 0.6 % as the *S* changes from 1120 rpm to 1600 rpm. A higher *S* increases the welding engagement, leading to higher heat generation at the interfaces. The hardness and strength of the two materials decrease, which increases the degree of the mixture; hence, the stir zone size and the bonded area enhances. Consequently, the tensile strength improves, leading to higher jointing efficiency. In contrast, a further *S* causes excessive heat input, which results in grain growth in the welded region. The tensile strength of the weld decreases, leading to a reduction in the *JE*. The similar influences of the *S* on the tensile strength can be found in the works of [1], [2], [4] and [6].

As shown in Fig. 10a, a higher *f* decreases the *JE*. When the *f* rises from 47 mm/min to 112 mm/min, the *JE* is relatively reduced by 15.73 %. A higher *f* increases the velocity of the welding tool and decreases the processing time. The heat generation at

the interfaces decreases, resulting in the lack of proper diffusion between the two plates. In other words, the degree of the mixture decreases, leading to higher grain size in the welded region. The tensile strength of the weld decreases, leading to a decreased *JE*. A reduction in the tensile strength with higher welding speed can be found in the works of [1], [2], [4], and [11].

a)

b)
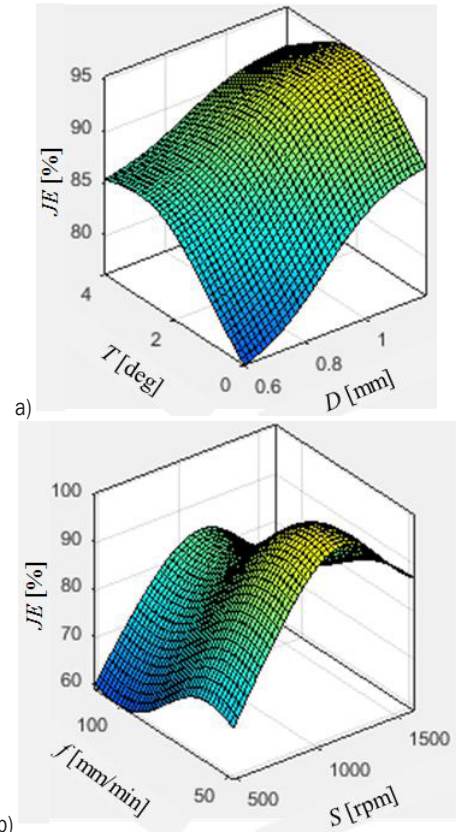
Fig. 10. *The interactive influences; a) JE versus S and f; and b) JE versus T and D*

Fig. 10b indicates that an increase in the *D* increases the *JE*. When the *D* relatively rises from 0.6 mm to 1.2 mm, the *JE* is relatively increased by 13.9 %. A higher depth of shoulder inside the workpiece is obtained with an increased *D*. An increase in the heat generation is obtained due to higher friction at the interfaces between the tool and workpiece increases. The consolidation of the weld by effective diffusion of atoms between the two plates is enhanced. A better mixture between two materials is achieved, leading to higher tensile strength; hence, the *JE* increases. Higher tensile strength with an increase in the depth of penetration can be found in the publications [8], [9], and [11].

As shown in Fig. 10b, the *JE* increases as the *T* increases to the middle value and decreases thereon. When the *T* rises from 0 deg to 2 deg, the *JE* is relatively increased by 10.1 %. The *JE* is relatively decreased by 3.9 % as the tool tile angle changes from 2 deg to 4 deg. A higher *T* causes an increased depth of shoulder inside the specimen; which leads to higher friction between the tool and workpiece. The heat generation increases at the interfaces, leading to a better mixture between two materials due to the enlargement in the welded zone. Therefore, the tensile strength of the joint increases, resulting in a higher *JE*. Further *T* causes excessive heat generation, leading to a coarse grain; hence, the *JE* decreases. The similar impacts of the tool title angle on the tensile strength are presented in the works of [3], [6], [16], and [18].

The influences of FSW parameters on the micro-hardness at the welded zone are shown in Fig. 11. As shown in Fig. 11a, a higher *S* decreases the *MH*. When the *S* relatively rises from 480 rpm to 1600 rpm, the *MH* is relatively reduced by 21.8 %. An increased *S* causes higher welding engagement at the interfaces between the tool and specimen. A higher degree of friction increases, leading to an increased heat generation in the welding region. The hardness and strength of the welded specimen decrease, resulting in soft and flexible structures; hence, the *MH* decreases. A decreased micro-hardness with higher welding speed can be found in the works of [2], [9], [12], and [15].

As shown in Fig. 11a, a higher *f* increases the *MH*. When the *f* relatively rises from 47 mm/min to 112 mm/min, the *MH* is relatively enhanced by 19.3 %. Higher *f* causes an increased velocity of the tool and a reduction in the welding time. The welding engagement decreases, leading to a reduction in the friction at the interfaces. The heat generation decreases, resulting in higher strength and hardness of the welded specimen. Therefore, an increased *MH* is obtained. Similar impacts of the welding speed on the micro-hardness are presented in the works of [2] and [12].

As shown in Fig. 11b, the *MH* decreases with an increased *D*. When the *D* relatively rises from 0.6 mm to 1.2 mm, the *MH* is relatively decreased by 15.9 %. A higher *D* increases the depth of the shoulder inside the workpiece. The friction at the interfaces between the tool and workpiece to be machined increases. Excessive heat generation is obtained, which causes the coarse-graining in welding metal and dissolves of sediments in aluminium alloys. Consequently, the *MH* decreases. Low micro-hardness with higher depth of penetration can be found in the works of [7] and [8].

As shown in Fig. 11b, the *MH* decreases with an increased *T*. When the *T* relatively rises from 0 deg to 4 deg, the *MH* is relatively decreased by 11.7 %. At a higher *T*, the depth of shoulder inside the specimen increases; which leads to higher friction between the tool and workpiece. The heat generation increases at the interfaces, leading to a higher grain size at the welded region. Consequently, low *MH* is observed with an increased *T*. The similar impacts of the tool title angle on the micro-hardness are presented in the works of [10] and [15].
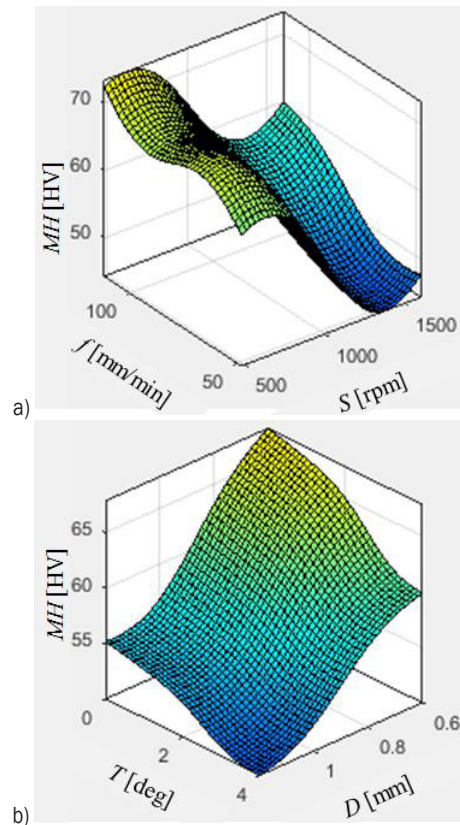
Fig. 11. *The interactive influences, a) EL versus S and f, and b) EL versus T and D*

3.4 Optimization Results

The developed ANFIS models are applied to select the optimal outcomes with the aid of the NCGA. The operating parameters of the NCGA are shown in Table 8. In this study, we select the collapse of the population (α) as the convergence parameter, which can be expressed as:

$$\alpha = \left(\frac{y_{\max} - y_{\min}}{y_{\max}} \right) \times 100, \qquad (13)$$

where y_{max} and y_{min} are the maximum and minimum responses.

Table 8. *Operating parameters of the NCGA*

No.	Symbol	Parameters	Values		
1	PO	Population size	20	40	60
2	NG	Number of generations	20	40	60
3	MR	Mutation rate	0.01	0.03	0.05
4	GS	Gene size	40	60	80
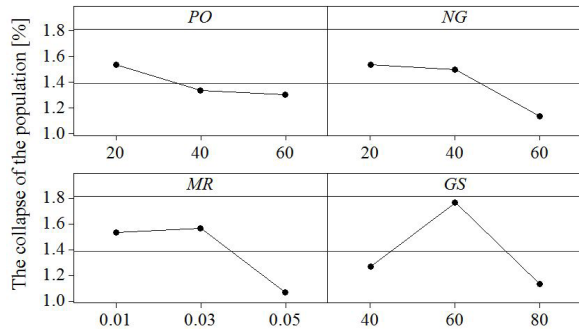
Fig. 12. *Selection of optimal NCGA parameters*

The minimum value of the α is utilized to select the convergence, while the *SWE* is considered as the objective function. The computation trials are conducted by means of the Taguchi experimental matrix L9. As shown in Fig. 12, the optimal data of the *PO*, *NG*, *MR*, and *GS* are 60, 60, 0.05, and 80, respectively.

We have simultaneously performed the PSO to solve the optimization issue. The Pareto graphs produced by the NCGA and PSO are presented in Figs. 13a and b, respectively. As a result, the number of feasible designs of the NCGA and PSO are 560 and 301, respectively. Moreover, the NCGA provides better results, as compared to the PSO ones (Table 9).

An experimental confirmation is conducted at the optimal point to check the reliability of the obtained results. The small deviation indicates that the proposed approach comprising the ANFIS, Taguchi method, and NCGA is feasible and reliable (Table 10).

The microstructure in the nugget zone is shown in Fig. 14, in which the grains are entirely transformed into fine-sized structure with even distribution and equal space. The welding defects, such as porosity, voids, flash, and cracks, have not been found in the welded zones. It can be stated that the fine grains using the recrystallization have been produced with the aid of optimal FSW parameters. In other words, the joints of AA6061 plates have been successfully implemented, leading to high-quality joint.
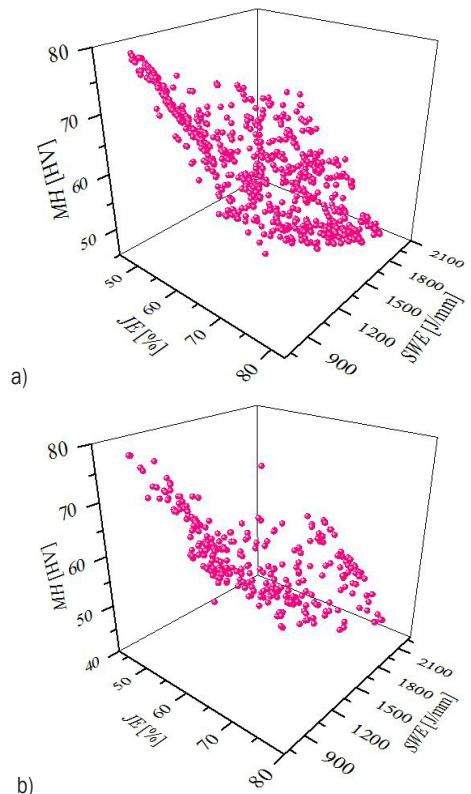
Fig. 13. *Pareto fronts; a) produced by the NCGA, b) produced by the PSO*
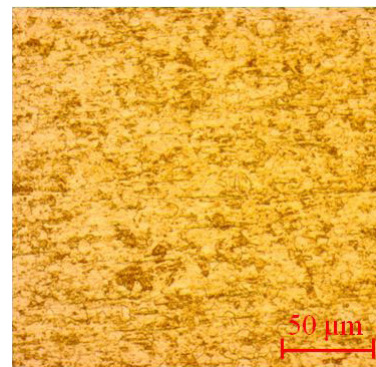
Fig. 14. *The microstructure in the nugget zone*

The industrial values can be listed as follows.

The obtained results are effectively applied to improve performance measures of the FSW process of the aluminium alloy.

The 2-2-2-2-2 ANFIS architectures could be used to render the relations between FSW parameters and the welding performances. The welding models proposed by the ANFIS approach are significant and adequate, which are capable of generating accurate predictions for the response values of the FSW operation of the aluminium alloy.

Table 9. *Optimization results generated by the NCGA and PSO*

Method	Optimization parameters				Responses		
	S [rpm]	f [mm/min]	D [mm]	T [deg]	EW [kJ]	JE [%]	MH [HV]
Initial values	480	77	0.9	4	1255.47	62.78	62.8
Optimal results-PSO	1040	85	0.8	3	1090.21	61.73	63.8
Optimal results-NCGA	560	90	0.9	2	1042.63	64.21	66.8
Improvement [%]					-17.0	2.3	6.4

Table 10. *Confirmatory results*

Method	Optimization parameters				Responses		
	S [rpm]	f [mm/min]	D [mm]	T [deg]	EW [kJ]	JE [%]	MH [HV]
Optimal results	560	90	0.9	2	1042.63	64.21	66.8
Experiment	560	90	0.9	2	1048.38	64.96	68.2
Error [%]					-0.6	-1.2	-2.1

4 CONCLUSIONS

In the current investigation, the friction stir welding (FSW) operation of the AA6061 has been addressed and optimized to decrease the specific welding energy (S*WE*) and enhance the jointing efficiency (*JE*) as well as the micro-hardness (*MH*). The optimizing FSW parameters are the rotational speed (*S*), welding speed (*f*), depth of penetration (*D*), and tool title angle (*T*). The ANFIS models of the welding responses were proposed in terms of the optimizing inputs, in which optimal operating parameters were optimized using the Taguchi method. The NCGA was applied to determine optimal values of welding parameters and objectives. The finding can be listed as follows.

1. The lowest levels of the *S*, *D*, and *T* could be utilized to reduce the *SWE*, while the highest *f* was recommended. To enhance the *JE*, higher values of the *S*, *D*, and *T* could be utilized, while lower *f* could be applied. Similarly, an increased *MH* could be obtained with higher values of the *S*, *D*, and *T*, while a lower *f* is encouraged.
2. All machining factors have significant contributions to the ANFIS models. For the *SWE* model, the *f* was named as the most effective factor, followed by the *S*, *D*, and *T*, respectively. For the *JE* model, the welding speed was the most effective factor, followed by the *D*, *S*, and *T*, respectively. For the *MH* model, the *S* had the highest contribution, followed by the *f*, *D*, and *T*, respectively.
3. The optimal parameters proposed by orthogonal array-based ANFIS-Taguchi method-NCGA of the *S*, *f*, *D*, and *T* were 560 rpm, 90 mm/min, 0.9 mm, and 2 deg, respectively. The *SWE* was

decreased by 17 %, while the *JE* and *MH* were enhanced by 2.3 % and 6.4 %, respectively.
4. This investigation addressed the specific welding energy, jointing efficiency, and micro-hardness at the welded zone under the variation of FSW parameters. The impacts of welding conditions on the costs and grain size will be explored in future works.
5. Practically, the weights reflect the importance of each response in relation to other performances. Therefore, the weight should be objectively determined based on experimental data, instead subjective chosen of the decisive maker to generate reliable optimal outcomes.

5 ACKNOWLEDGEMENTS

6 REFERENCES

[1] Kasman, Ş. (2013). Multi-response optimization using the Taguchi-based grey relational analysis: a case study for dissimilar friction stir butt welding of AA6082-T6/AA5754-H111. The International Journal of Advanced Manufacturing Technology, vol. 68, p. 795-804, **DOI:10.1007/s00170-012-4720-0.**

[2] Babajanzade Roshan, S., Behboodi Jooibari, M., Teimouri, R., Asgharzadeh-Ahmadi, G., Falahati-Naghibi, M., Sohrabpoor, H., (2013). Optimization of friction stir welding process of AA7075 aluminum alloy to achieve desirable mechanical properties using ANFIS models and simulated annealing algorithm. *The International Journal of Advanced Manufacturing Technology*, vol. 69, p. 1803-1818, **DOI:10.1007/s00170-013-5131-6.**

[3] Ahmadi, H., Mostafa Arab, N.B., Ghasemi, F.A. (2014). Optimization of process parameters for friction stir lap welding of carbon fibre reinforced thermoplastic composites by Taguchi method. *Journal of Mechanical Science and Technology*, vol. 28, p. 279-284, **DOI:10.1007/s12206-013-0966-1**.

[4] Shojaeefard, M.H., Akbari, M., Asadi, P. (2014). Multi objective optimization of friction stir welding parameters using FEM and neural network. *International Journal of Precision Engineering and Manufacturing*, vol. 15, p. 2351-2356, **DOI:10.1007/s12541-014-0600-x**.

[5] Senthilraja, R., Sait, A.N. (2015). Optimization of the parameters of friction stir welding for AZ91D magnesium alloy using the Taguchi Design. *Materials Science*, vol. 51, p. 180-187, **DOI:10.1007/s11003-015-9826-8**.

[6] Kumar, S., Kumar, S. (2015) Multi-response optimization of process parameters for friction stir welding of joining dissimilar Al alloys by gray relation analysis and Taguchi method. *Journal of the Brazilian Society of Mechanical Sciences and Engineering*, vol. 37, p. 665-674, **DOI:10.1007/s40430-014-0195-2**.

[7] Guo, C., Shen, Y., Hou, W., Yan, Y., Huang, G., Liu, W. (2018). Effect of groove depth and plunge depth on microstructure and mechanical properties of friction stir butt welded AA6061-T6. *Journal of Adhesion Science and Technology*, vol. 32, p. 2709-2726, **DOI:10.1080/01694243.2018.1505347**.

[8] Saju, T.P., Narayanan, G.R. (2018). Effect of tool plunge depth on joint formation and mechanical performance of friction stir forming joints made between AA 5052-H32 and AA 6061-T6 sheet metals. *Transactions of Nonferrous Metals Society of China*, vol. 28, no. 4, p. 613-628, **DOI:10.1016/S1003-6326(18)64694-1**.

[9] Siddharth, S., Senthilkumar, T. (2016). Optimization of friction stir spot welding process parameters of dissimilar Al 5083 and C 10100 joints using response surface methodology. *Russian Journal of Non-Ferrous Metals*, vol. 57, p. 456-466, **DOI:10.3103/S1067821216050151**.

[10] Elyasi, M., Aghajani Derazkola, H., Hosseinzadeh, M. (2016). Investigations of tool tilt angle on properties friction stir welding of A441 AISI to AA1100 aluminium. *Proceedings of the Institution of Mechanical Engineers, Part B: Journal of Engineering Manufacture*, vol. 230, no. 7, p. 1234-1241, **DOI:10.1177/0954405416645986**.

[11] Farzadi, A., Bahmani, M., Haghshenas, D.F. (2017). Optimization of operational parameters in friction stir welding of AA7075-T6 aluminum alloy using response surface method. *Arabian Journal for Science and Engineering*, vol. 42, p. 4905-4916, **DOI:10.1007/s13369-017-2741-6**.

[12] Gupta, S.K., Pandey, K.N., Kumar, R. (2018). Multi-objective optimization of friction stir welding process parameters for joining of dissimilar AA5083/AA6063 aluminum alloys using hybrid approach. *Proceedings of the Institution of Mechanical Engineers, Part L: Journal of Materials: Design and Applications*, vol. 232, no. 4, p. 343-353, **DOI:10.1177/1464420715627294**.

[13] Palanivel, R., Laubscher, R., Vigneshwaran, S., Dinaharan, I. (2018). Prediction and optimization of the mechanical properties of dissimilar friction stir welding of aluminum alloys using design of experiments. *Proceedings of the Institution of Mechanical Engineers, Part B: Journal of Engineering Manufacture*, vol. 232, no. 8, p. 1384-1394, **DOI:10.1177/0954405416667404**.

[14] D'Orazio, A., Forcellese, A., Simoncini, M. (2019). Prediction of the vertical force during FSW of AZ31 magnesium alloy sheets using an artificial neural network-based model. *Neural Computing & Applications*, vol. 31, p. 7211-7226, **DOI:10.1007/s00521-018-3562-6**.

[15] Rajendran, C., Srinivasan, K., Balasubramanian, V., Balaji, H., Selvaraj, P. (2019). Effect of tool tilt angle on strength and microstructural characteristics of friction stir welded lap joints of AA2014-T6 aluminum alloy. *Transactions of Nonferrous Metals Society of China*, vol. 29, no. 9, p. 1824-1835, **DOI:10.1016/S1003-6326(19)65090-9**.

[16] Kamal Babu, K., Panneerselvam, K., Sathiya, P., Noorul Haq, A., Sundarrajan, S., Mastanaiah, P., Srinivasa Murthy, C.V. (2018). Parameter optimization of friction stir welding of cryorolled AA2219 alloy using artificial neural network modeling with genetic algorithm. *The International Journal of Advanced Manufacturing Technology*, vol. 94, p. 3117-3129, **DOI: 10.1007/s00170-017-0897-6**.

[17] Senthil, S.M., Parameshwaran, R., Ragu Nathan, S., Bhuvanesh Kumar, M., Deepandurai, K. (2020). A multi-objective optimization of the friction stir welding process using RSM-based-desirability function approach for joining aluminum alloy 6063-T6 pipes. *Structural and Multidisciplinary Optimization*, vol. 62, p. 1117-1133, **DOI:10.1007/s00158-020-02542-2**.

[18] Verma S, Kumar V. (2021). Optimization of friction stir welding parameters of dissimilar aluminium alloys 6061 and 5083 by using response surface methodology. *Proceedings of the Institution of Mechanical Engineers, Part C: Journal of Mechanical Engineering*, **DOI:10.1177/09544062211005804**.

[19] Boukraa, M., Chekifi, T., Lebaal, N., Aissani, M. (2021). Robust optimization of both dissolution time and heat affected zone over the friction stir welding process using SQP technique. *Experimental Techniques*, **DOI:10.1007/s40799-021-00515-8**.

[20] Satheesh, C., Sevvel, P., Senthil Kumar, R. (2020). Experimental identification of optimized process parameters for FSW of AZ91C Mg alloy using quadratic regression models. *Strojniški vestnik - Journal of Mechanical Engineering*, vol. 66, no. 12, p. 736-751, **DOI:10.5545/sv-jme.2020.6929**.

[21] Sevvel, P., Dhanesh Babu, S.D., Senthil Kumar, R. (2020). Peak temperature correlation and temperature distribution during joining of AZ80A Mg alloy by FSW - a numerical and experimental investigation. *Strojniški vestnik - Journal of Mechanical Engineering*, vol. 66, no. 6, p. 395-407, **DOI:10.5545/sv-jme.2020.6566**.

[22] Bhatia, A., Wattal, R. (2021). Process parameters optimization for maximizing tensile strength in friction stir-welded carbon steel. *Strojniški vestnik - Journal of Mechanical Engineering*, vol. 67, no. 6, p. 311-321, **DOI:10.5545/sv-jme.2021.7203**.

[23] Dhanesh Babu, S.D., Sevvel, P., Senthil Kumar, R. (2020). Simulation of heat transfer and analysis of impact of tool pin geometry and tool speed during friction stir welding of AZ80A Mg alloy plates. *Journal of Mechanical Science and Technology*, vol. 34, p. 4239-4250, **DOI:10.1007/s12206-020-0916-7**.

[24] Ho, W.H., Tsai, J.T., Lin, B.T., Chou, J.H. (2009). Adaptive network-based fuzzy inference system for prediction of surface roughness in end milling process using hybrid Taguchi-genetic learning algorithm. *Expert Systems with Applications*, vol. 36, no. 2, p. 3216-3222, **DOI:10.1016/j.eswa.2008.01.051**.

[25] Warsi, S.S., Agha, M.H., Ahmad, R., Jaffery, S.H.I, Khan, M. (2019). Sustainable turning using multi-objective optimization: a study of Al 6061 T6 at high cutting speeds. *The International Journal of Advanced Manufacturing Technology*, vol. 100, p. 843-855, **DOI:10.1007/s00170-018-2759-2**.

[26] Jang, D.-Y.., Jung, J., Seok, J. (2016). Modeling and parameter optimization for cutting energy reduction in MQL milling process. *International Journal of Precision Engineering and Manufacturing-Green Technology*, vol. 3, p. 5-12, **DOI:10.1007/s40684-016-0001-y**.

[27] Teimouri, R. Amini, S. (2019). A comprehensive optimization of ultrasonic burnishing process regarding energy efficiency and workpiece quality. *Surface and Coatings Technology*, vol. 375, p. 229-242, **DOI:10.1016/j.surfcoat.2019.07.03**.